

Kondo Lattice Model with Finite Temperature Lanczos Method

I. Zerec,¹ B. Schmidt,² and P. Thalmeier²

¹Max-Planck-Institute for the Physics of Complex Systems, D-01187 Dresden, Germany

²Max-Planck-Institute for Chemical Physics of Solids, D-01187 Dresden, Germany

(Dated: December 2, 2024)

We investigate the Kondo Lattice Model on 2D clusters using the Finite Temperature Lanczos Method. The temperature dependence of thermodynamic and correlations functions are systematically studied for various Kondo couplings J_K . The ground state values for the total local moment is presented as well. Finally, the phase diagrams of the finite clusters are constructed for the periodic and open boundary conditions. For the two boundary conditions, two different regimes are found for small J_K/t , depending on the distribution of non-interacting conduction electron states. If there are states within J_K around the Fermi level, the two energy scales, linear and quadratic in J_K , exist. The former is associated with the onsite screening and the latter with the RKKY interaction. If there are no states within J_K around the Fermi level, the only energy scale is that of the RKKY interaction. The results imply that the form of the electron density of states (DOS) plays an important role in the competition between the Kondo screening and the RKKY interaction. The former is stronger if the DOS is larger around the Fermi level, while the latter is less sensitive to the form of the DOS.

PACS numbers: 62.30.+d,65.40.-b,66.35.+a

I. INTRODUCTION

The Kondo lattice model (KLM) is used to describe compounds containing localized magnetic moments, such as heavy fermion systems and Kondo insulators.¹ The KLM Hamiltonian is given by:

$$H_{KL} = -t \sum_{i,j;\sigma} c_{i,\sigma}^\dagger c_{j,\sigma} + J_K \sum_i \boldsymbol{\tau}_i \cdot \mathbf{S}_i. \quad (1)$$

Here, $\boldsymbol{\tau}_i$ and \mathbf{S}_i are the itinerant and the local (f -) spin on site i , respectively. The KLM takes into account hopping of conduction electrons, t , and their Kondo interaction, J_K , with local f -spins. The Kondo term causes the screening of local spins, but also induces the indirect RKKY interaction between the local spins on the lattice. These two interactions compete, leading to either magnetically ordered or non-magnetic ground state, separated by the quantum critical point (QCP).² The nature of the QCP in heavy fermion compounds is one of the central topics of condensed matter physics today.^{3,4,5,6,7,8,9,10}

Various analytical and numerical methods have been used to study the KLM, like the mean-field approach¹¹ and the Quantum Monte Carlo (QMC) method.¹² The finite temperature Lanczos method (FTLM)¹³ has been used to study the thermodynamic functions.¹⁴ Also the periodic Anderson model on finite size clusters has been studied with similar method recently.¹⁵

Here, we use the FTLM and mainly focus the analysis on the temperature dependence and the ground state values of the static correlation functions, of central importance for the QCP. We consider onsite vs. intersite correlations for the lattice and also compare the former with the impurity case. The latter is associated with the RKKY interaction. We also investigate the evolution of the total onsite moment with Kondo coupling strength

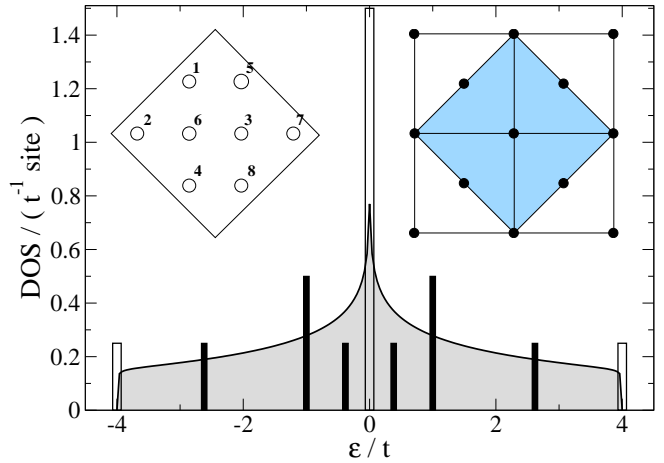


FIG. 1: The DOS for the tight-binding model in 2D is shown shaded. Unshaded bars represent discrete levels of 2D 8-site cluster (for $J_K = 0$) with PBC. The black bars represent levels with OBC. The bar heights correspond to the level degeneracy (divided by 8). Left Inset: The 8-site cluster with site indices. Right Inset: The first Brillouin zone with the k -points corresponding to the Bloch states of 8-site cluster. The shaded part represents the Fermi volume for half filled case. There are 6 degenerate states on the "Fermi surface" when the multiplicities are taken into account correctly.

J_K . The main advantage of the FTLM is that it involves no uncontrolled approximations and is exact for finite size clusters. It treats both, the Kondo screening and the RKKY interaction, correctly.

We consider the 8-site cluster of a square lattice, as shown in the inset of Fig. 1, with periodic (PBC) and open (OBC) boundary conditions at half filling.

We will show that for this cluster the two different boundary conditions lead to two interesting physical sit-

ulations, which may have relevance to the two types of QCP's observed. There is of course only one solution of the KLM in the thermodynamic limit, but the real materials have more complex band structure. By varying boundary conditions for the simple model on the small cluster one may mimic band structures with different characteristic behaviour of the density of states (DOS) around the Fermi level. For this reason we present in detail the analysis of the KLM on the finite cluster for the PBC and the OBC and compare the two cases. In Sec. II we discuss the specific heat anomalies obtained in the two cases. Sec. III discusses the central problem of Kondo-lattice physics: The competition and crossover behaviour of onsite and intersite correlations as function of temperature and control parameter J_K/t . The associated Kondo screening behaviour evident from the susceptibility and total local moment is presented in Sec. IV. Finally Sec. V summarizes the results in a phase diagram and gives the conclusions.

II. THE SPECIFIC HEAT

The specific heat for the PBC and the OBC, for various coupling constants J_K , is shown in Fig. 2.

The low-temperature specific heat for the non-interacting case, $J_K = 0$, with PBC deviates significantly from the thermodynamic limit. The reason is that 6 out of 8 electrons are placed on the "Fermi surface", shown in the inset of Fig. 1, thus the ground state is highly degenerate. The specific heat for the OBC is closer to the thermodynamic limit. The peak from the hopping term for $J_K = 0$ is much more pronounced and at lower temperature, $T_{\max,0}^{\text{OBC}}$, for the OBC than for the PBC. The electronic states for the OBC are no longer Bloch states, but the important point is that the electron energies are shifted from, and distributed below, the "Fermi level". The distribution of these discrete levels is such that it relatively well mimics the continuum DOS in the thermodynamic limit, as shown in Fig. 1.

The specific heat for the PBC and the OBC, when the Kondo interaction is turned on, shows qualitatively different behavior in the weak coupling regime, $J_K/t \lesssim 2$, as shown in Fig. 2. For the PBC, a double peak structure is observed at low temperatures for $0.5 < J_K/t \lesssim 2$. We may denote the positions of the upper and the lower peak by $T_{\max,1}^{\text{PBC}}$ and $T_{\max,2}^{\text{PBC}}$, respectively. For the OBC only one low temperature peak appears at $T_{\max,1}^{\text{OBC}}$. The origin of these peaks are spin degrees of freedom, whose degeneracy is lifted by the Kondo interaction. In the strong coupling limit there is only one peak in the specific heat, and it does not depend on the boundary conditions.

The specific heat for the OBC agrees with the results obtained with the same method for the 10-site cluster with the PBC in Ref. 14, as well as with the results obtained with the QMC in Ref. 12.

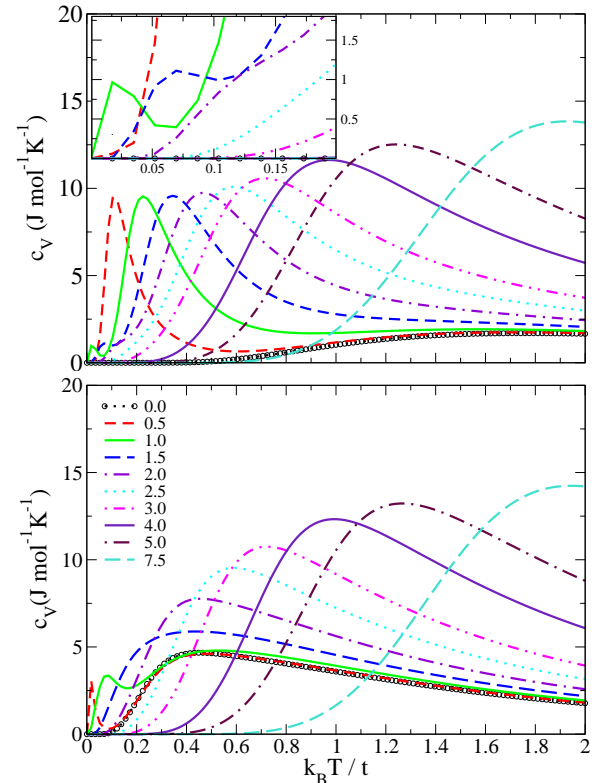


FIG. 2: (Color online) The specific heat calculated for various values of J_K/t , as indicated in the legend. The legend is valid for all the figures in this work, if not explicitly specified. Above: The PBC. The two low temperature peaks can be seen for $0.5 < J_K/t \lesssim 2$. In the inset the lower peaks are magnified. Below: The OBC. The $J_K/t = 0$ curve agrees well with the thermodynamic limit of the Hamiltonian (1). For $J_K/t > 0$ there is only one low temperature peak.

III. SPIN CORRELATION FUNCTIONS: ONSITE SINGLET FORMATION VS. RKKY INTERACTIONS

The nature of the specific heat peaks may be revealed by considering appropriate static correlation functions. We focus the analysis on the following two: $\langle \tau_1 \cdot \mathbf{S}_1 \rangle$ is the onsite correlation function between the local and the itinerant spin, while $\langle \mathbf{S}_1 \cdot \mathbf{S}_5 \rangle$ is the intersite correlation function between the local spins on the neighboring sites for the PBC. For the OBC these are $\langle \tau_3 \cdot \mathbf{S}_3 \rangle$ and $\langle \mathbf{S}_3 \cdot \mathbf{S}_6 \rangle$, i.e., the inner sites 3 and 6 are considered, because they are more representative than the sites on the edges of the cluster (cf. Fig. 1).

A. Periodic Boundary Conditions

The onsite correlations, $\langle \tau_1 \cdot \mathbf{S}_1 \rangle$, for the PBC as function of temperature are shown in Fig. 3. They are also compared with the onsite correlations for the impurity

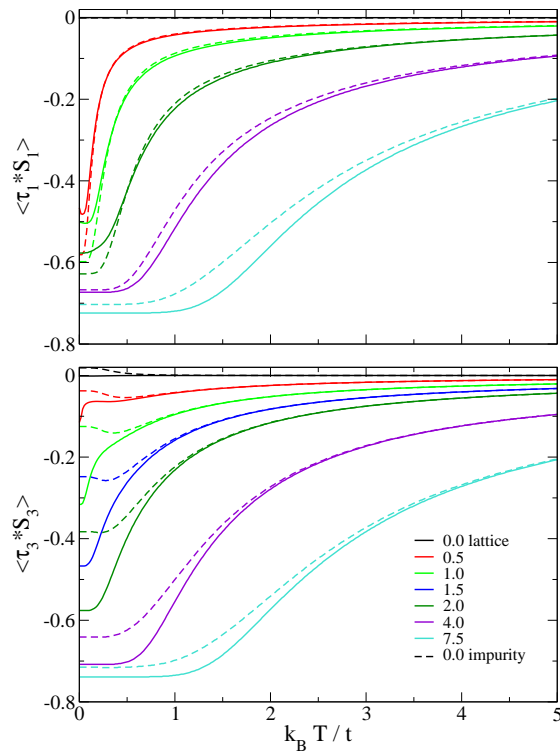


FIG. 3: (Color online) The onsite correlations in the lattice (full lines) as function of temperature and the comparison with the impurity case (broken lines), for J_K/t values as indicated in the legend. The correlation strength increases monotonically with increasing J_K/t . In the impurity case, the impurity local spin is placed on site 1 for the PBC, and site 3 for the OBC. Above: The PBC. Below: The OBC. Due to the small system size for the impurity case, there are some unphysical deviations at low temperatures and weak coupling J_K/t for the OBC.

case, where there is only one local spin, at site 1, on the 8-site cluster. In the weak coupling regime the onsite screening is decreased in the lattice, because there are less itinerant spins per local spin available for the screening.

The inflection points of the correlation functions, as function of temperature, indicate that the upper peak in the specific heat, at $T_{\max,1}^{\text{PBC}}$, corresponds to the formation of the onsite correlations, whereas the lower one, at $T_{\max,2}^{\text{PBC}}$, corresponds to the formation of the intersite correlations. The ground state ($T = 0$ K) correlations for the PBC as function of the coupling J_K/t are shown in the inset of Fig. 4. It is seen that the onsite correlations are stronger than the intersite correlations for all J_K/t . Another characteristic is that $\langle \tau_1 \cdot S_1 \rangle$ jumps to the large absolute value as soon as J_K is turned on. It is a consequence of the degenerate itinerant degrees of freedom at Fermi level for $J_K = 0$. The free itinerant spins on the "Fermi level" screen the local spins onsite as soon as $J_K > 0$. The ground state splits off and is characterized

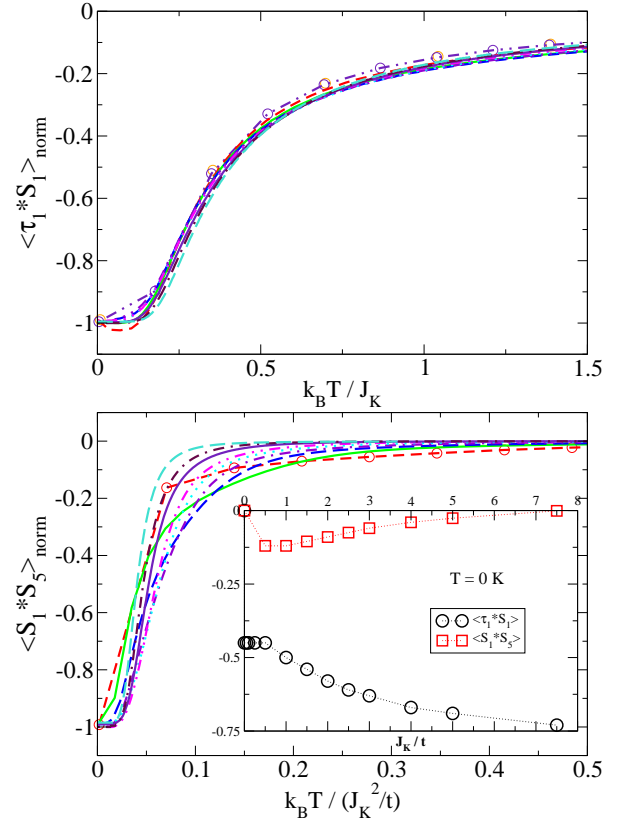


FIG. 4: (Color online) Correlation functions for the PBC. Above: Normalized $\langle \tau_1 \cdot S_1 \rangle$ as function of temperature divided by J_K . Below: Normalized $\langle S_1 \cdot S_5 \rangle$ as function of temperature divided by the square of J_K . The normalization is achieved by dividing the curves with the ground state values. In the Inset the ground state ($T = 0$ K) correlations as function of J_K/t are shown.

by finite $\langle \tau_1 \cdot S_1 \rangle$ correlations. The unscreened parts of the local spins form intersite correlations, $\langle S_1 \cdot S_5 \rangle$, below $T_{\max,2}^{\text{PBC}}$, due to the RKKY interaction. The $\langle S_1 \cdot S_5 \rangle$ increases rapidly as J_K is turned on. Because of the very small energy scale (quadratic in J_K), convergence problems appear in the calculation of ground state $\langle S_1 \cdot S_5 \rangle$ correlations for $J_K/t < 0.5$ and we were not able to determine whether they also jump for finite J_K . In the strong coupling regime the intersite correlations vanish, while the onsite correlations saturate at $-3/4$, as the onsite singlets are formed.

The correlation functions, normalized to the ground state values, versus scaled temperature, as done in Ref. 12, are shown in Fig. 4. The onsite correlations are characterized by a single temperature scale, perfectly linear in J_K/t . The intersite correlations are also characterized by a single temperature scale proportional to the J_K^2/t . This shows that for the PBC the onsite screening is independent of the intersite correlations, which may be associated with the RKKY interaction. This is a consequence of the special symmetry of the 8-site cluster lead-

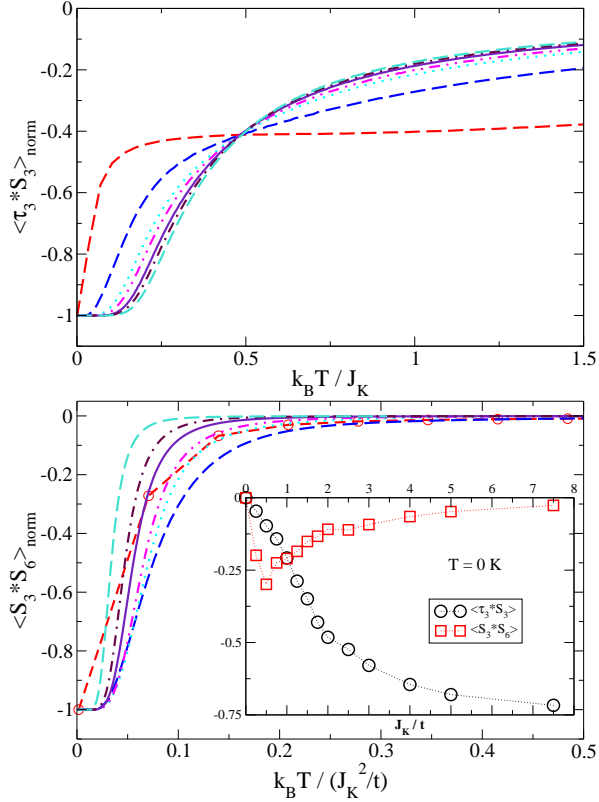


FIG. 5: (Color online) Correlation functions for the OBC. Above: Normalized $\langle \tau_3 \cdot S_3 \rangle$ as function of temperature divided by J_K . Below: Normalized $\langle S_3 \cdot S_6 \rangle$ as function of temperature divided by J_K^2/t . The normalization is achieved by dividing the curves with the ground state values. In the Inset the ground state ($T = 0$ K) correlations as function of J_K/t are shown.

ing to the large fraction of conduction electron sitting on the "Fermi surface". Nevertheless it is an interesting result which may have relevance for a case where the conduction electron DOS is strongly peaked at the Fermi level.

B. Open Boundary Conditions

The onsite correlations, $\langle \tau_3 \cdot S_3 \rangle$, for the OBC as function of temperature and the comparison to the impurity case are also shown in Fig. 3. In contrast to the PBC, for the OBC the onsite correlations are enhanced in the lattice. In the case of OBC there are no "free" itinerant spins, i.e., conduction electrons on the "Fermi level". In the weak coupling limit the onsite screening is not a direct process and is weak. The interesting point is the appearance of a new low energy scale in the lattice, which may be noted as a low-temperature downturn in the onsite correlations on Fig. 3.

The ground state correlations are shown in the inset of Fig. 5. The onsite correlations, $\langle \tau_3 \cdot S_3 \rangle$, do not

jump as J_K is turned on, but rather increase continuously with J_K . The intersite correlations, $\langle S_3 \cdot S_6 \rangle$, are much stronger than $\langle S_1 \cdot S_5 \rangle$ for the PBC and in the weak coupling limit they are even larger in absolute values than the onsite $\langle \tau_3 \cdot S_3 \rangle$ correlations. It is understandable, because the local spins are only weakly screened, due to the lack of the "free" itinerant spins. Therefore, the unscreened local spins form strong intersite correlations.

The normalized correlations as function of the scaled temperature for the OBC are shown in Fig. 5. The $\langle \tau_3 \cdot S_3 \rangle$ scale with J_K only in the strong coupling limit. In the weak coupling limit the two characteristic temperatures or energy scales can be identified, as already mentioned above. The upper one is associated with the energy splitting of the discrete energy levels (cf. Fig. 1), and is clearly a finite size effect. The lower energy scale is associated with the additional onsite screening, due to the presence of other local spins in the lattice. The intersite $\langle S_3 \cdot S_6 \rangle$ correlations are still approximately governed by a single energy scale, J_K^2/t , just as for the PBC. Indeed the behavior of the normalized intersite correlation functions for the OBC and the PBC are quite similar, despite of the fact that the magnitude differs by a factor of two.

IV. MAGNETIC SUSCEPTIBILITY AND TOTAL LOCAL MAGNETIC MOMENT

The spin correlations are also directly reflected in the magnetic susceptibility, shown in Fig. 6, for the PBC and the OBC. It is multiplied by J_K and plotted versus temperature scaled with J_K , as was done in Ref. 12. The two peaks for the PBC are clearly seen for small J_K/t , as in the specific heat. However, in the magnetic susceptibility even the lower peak for $J_K/t = 0.5$ is clearly seen. This is because the lower peaks in the magnetic susceptibility are much more pronounced and at slightly higher temperatures than the corresponding peaks in the specific heat. The position of the lower peak scales well with J_K^2 (not shown in the figure). The lower peak is not distinguishable any more for $J_K/t \gtrsim 2$. The position of the higher peak scales with J_K . For the OBC only one large peak is seen. For $J_K/t \lesssim 2$ it scales approximately with J_K^2 . In the strong coupling limit, $J_K/t \gtrsim 2$, the peak scales linearly with J_K , just as for the PBC. The results for the OBC are similar to the results for the 10-site cluster with PBC in Ref. 14. These results are also similar to the results of the QMC calculations for larger clusters in Ref. 12. However, in Ref. 12, the magnetic susceptibility peak scales with J_K^2 , while in the onsite correlations the characteristic temperature is proportional to J_K , suggesting the existence of the two low energy scales.

In the insets of Fig. 6 the ground state values of the total local moments are shown, defined as:

$$\langle \mu_{\text{loc}}^2 \rangle = \langle (\tau_i + S_i)^2 \rangle = \langle \tau_i^2 \rangle + \langle S_i^2 \rangle + 2\langle \tau_i \cdot S_i \rangle. \quad (2)$$

The interesting quantity here is $\langle \tau_i^2 \rangle$ which is the mea-

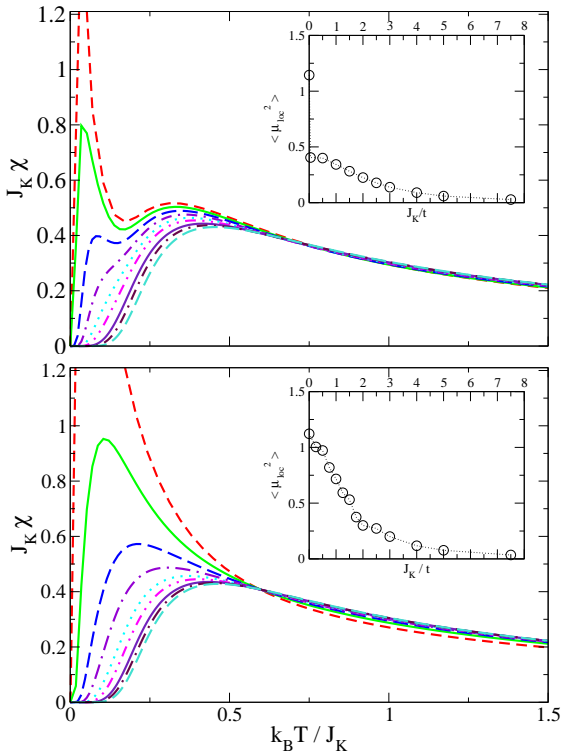


FIG. 6: (Color online) The scaled magnetic susceptibility, as indicated on the axes. Above: The PBC. Below: The OBC. In the Insets the total local moments in the ground state (at $T = 0$ K) as function of J_K/t are shown, $\langle \mu_{loc}^2 \rangle = \langle (\tau_i + \mathbf{S}_i)^2 \rangle$, ($i = 1, 3$ for the PBC and OBC, respectively).

sure of the localization of the itinerant spins. In the strong coupling limit $\langle \tau_i^2 \rangle = 3/4$, i.e., the itinerant spins become localized as the onsite singlets are formed and the hopping of conduction electrons is frozen. When the conduction electrons are completely delocalized, i.e., for $J_K = 0$, $\langle \tau_i^2 \rangle = 3/8$, because the probability of finding one electron with spin up or down on one particular site is 1/2. Accordingly, $\langle \mu_{loc}^2 \rangle = 9/8$ for $J_K = 0$ and it vanishes as the onsite singlets are formed and the local moments are completely screened, for $J_K \rightarrow \infty$. There is a jump for $J_K/t > 0$ for the PBC. It has the same origin as the jump for the onsite correlations $\langle \tau_1 \cdot \mathbf{S}_1 \rangle$, i.e., the highly degenerate unperturbed conduction electron ground state. A jump is also present in the $\langle \tau_i^2 \rangle$. For the OBC we see a continuous decrease of $\langle \mu_{loc}^2 \rangle$.

The $\langle \mu_{loc}^2 \rangle$ is a good quantity to define a critical value of J_K/t at which the crossover from predominantly magnetic to predominantly nonmagnetic state occurs. The other possibility would be to compare directly the intersite and onsite correlations, but the intersite correlations depend strongly on the cluster size. Therefore we define a critical $(J_K/t)_C$ as the value for which $\langle \mu_{loc}^2 \rangle = \langle \mu_{loc}^2 \rangle_0/2$. Then for the OBC, $(J_K/t)_C \approx 1.4$ (cf. Fig. 6), in good agreement with the values obtained from the Quantum

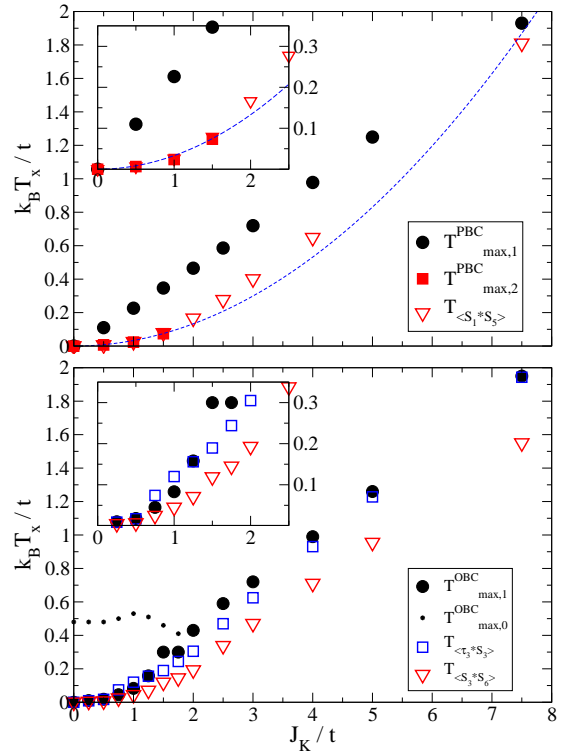


FIG. 7: (Color online) The phase diagrams for the 8-site 2D clusters. In the Insets the weak coupling region is magnified. Above: The PBC. The inflection points are approximately determined as the temperatures where the normalized $\langle \mathbf{S}_1 \cdot \mathbf{S}_5 \rangle$ has the value of -0.75. The dashed line is the fitting curve assuming quadratic dependence on J_K . The inflection points of the onsite correlations agree with the positions of the upper peak in the specific heat and are not shown in the Figure. Below: The OBC. The inflection points are approximately determined as the temperatures where the normalized correlation functions achieve the values of -0.8 and -0.75 for $\langle \tau_3 \cdot \mathbf{S}_3 \rangle$ and $\langle \mathbf{S}_3 \cdot \mathbf{S}_6 \rangle$, respectively.

Monte Carlo¹² and the mean-field analysis.¹⁶ For the PBC it would be 0, but for this small cluster size, the OBC are much more representative for the thermodynamic limit of the KLM given by eq. (1).

V. PHASE DIAGRAM AND CONCLUSIONS

We may summarize the results in form of the phase diagrams for the PBC and the OBC, shown in Fig. 7. In the phase diagrams the positions of the specific heat maxima are plotted as function of the coupling strength, J_K/t . Also the inflection points of the correlation functions are plotted, and they mostly follow the positions of the corresponding specific heat maxima.

In the weak coupling regime, for the PBC, the two characteristic temperatures $T_{max,1}^{PBC}$ and $T_{max,2}^{PBC}$ are found. The $T_{max,2}^{PBC}$ cannot be determined for $J_K/t \gtrsim 2$, but we

make the continuation with the $\langle \mathbf{S}_1 \cdot \mathbf{S}_5 \rangle$ inflection point temperature, $T_{\langle \mathbf{S}_1 \cdot \mathbf{S}_5 \rangle}$, which can be defined for all coupling strengths. Therefore we conclude that the corresponding anomaly in the specific heat is still there, but is too small to be identified. The inflection points of the correlation functions reveal that the characteristic temperatures $T_{\max,1}^{\text{PBC}}$ and $T_{\max,2}^{\text{PBC}}$ correspond to the energy scales of the onsite correlations and the intersite correlations, respectively. The former is linear in J_K for all J_K/t . The latter is proportional to J_K^2/t , and may be associated with the RKKY interaction.

For the OBC, there is only one characteristic temperature, $T_{\max,1}^{\text{OBC}}$, for all J_K/t . In the weak coupling regime, for $J_K/t \lesssim 2$, below $T_{\max,1}^{\text{OBC}}$ predominantly intersite correlations form. However, $T_{\max,1}^{\text{OBC}}$ is also the characteristic temperature of the onsite correlations. This is seen from the positions of the inflection points for the corresponding correlations, also shown in the lower part of Fig. 7. Because the intersite correlations dominate and the characteristic temperature is approximately quadratic in J_K , the corresponding energy scale, in the weak coupling regime, may be associated with the RKKY interaction.

It is important to note that $T_{\max,1}^{\text{OBC}} \approx T_{\max,2}^{\text{PBC}}$, i.e., the RKKY interaction is not very sensitive to the distribution of the non-interacting conduction electron states. This is plausible with the known expression for the RKKY characteristic temperature, $T_{\text{RKKY}} \propto J_K^2/W$ (e.g.⁴), where W is the band width. It is also important that the RKKY energy scale is the energy scale of the onsite correlations in the weak coupling regime for the OBC. We may generally conclude that the RKKY energy scale is the lowest energy scale of the KLM; if the local spins are not screened above T_{RKKY} , then it is the only energy scale of the system.

In contrast, the onsite correlations, i.e., the onsite screening of local spins, is very sensitive to the number of states within J_K around the "Fermi level", as seen from the difference between $T_{\max,1}^{\text{PBC}}$ and $T_{\max,1}^{\text{OBC}}$ for the PBC and the OBC, respectively. This is plausible with the expression for the single impurity Kondo temperature,

which depends exponentially on the DOS at the Fermi level, $\rho(\epsilon_F)$; $T_K = \epsilon_F \exp[-1/(J\rho(\epsilon_F))]$.

In the strong coupling regime, only one characteristic temperature is found for both, PBC and OBC. It corresponds to the energy of the onsite singlet formation, which is linear in J_K . Boundary conditions are unimportant, because the local physics determines the properties of the system.

We may argue on the relevance of these results for the system in the thermodynamic limit. Recently a QCP was found^{5,6,8} whose properties deviate from the expected behavior (e.g.^{9,10}). The properties of the system at the QCP are determined by the competition between the onsite screening and the RKKY interaction. Here we have shown that the competition between the onsite screening and the RKKY interaction strongly depends on the particular form of the distribution of the non-interacting conduction electron levels. We may anticipate that in the thermodynamic limit this means a strong dependence on the particular form of the non-interacting conduction electron DOS. A strongly peaked DOS near the Fermi level favors onsite screening, while the RKKY interaction is not very sensitive to the particular shape of the DOS. These results indicate that the shape of the DOS is very important for the properties of the heavy fermion systems in the vicinity of the QCP.

Finally, the qualitative behavior of the correlation functions for the KLM with OBC is similar to the KLM without charge degrees of freedom,¹⁷ which is the generalized Kondo necklace model in 2D from the Doniach's original work.² This shows that this simplified model describes well the spin degrees of freedom in the KLM at the half-filling.

Acknowledgments

We wish to acknowledge useful discussions with P. Fulde, S. Burdin, N. Perkins, and R. Ramazashvili.

¹ H. Tsunetsugu, M. Sigrist, and K. Ueda, Rev. Mod. Phys. **69**, 803 (1997).
² S. Doniach, Physica B **91**, 231 (1977).
³ J. Rech, P. Coleman, G. Zarand, and O. Parcollet, cond-mat/0507001.
⁴ P. Sun and G. Kotliar, Phys. Rev. Lett. **95**, 016402 (2005).
⁵ S. Paschen, T. Lühmann, S. Wirth, P. Gegenwart, O. Trovarelli, C. Geibel, F. Steglich, P. Coleman, and Q. Si, Nature **432**, 881 (2004).
⁶ J. Custers, P. Gegenwart, H. Wilhelm, K. Neumeier, Y. Tokiwa, O. Trovarelli, C. Geibel, F. Steglich, C. Pepin, and P. Coleman, Nature **424**, 524 (2003).
⁷ Q. Si, S. Rabello, K. Ingersent, and J. Smith, Nature **413**, 804 (2001).
⁸ A. Schröder, G. Aeppli, R. Coldea, M. Adams, O. Stockert,

H. Löhneysen, E. Bucher, R. Ramazashvili, and P. Coleman, Nature **407**, 351 (2000).
⁹ N. Mathur, F. Grosche, S. Julian, I. Walker, D. Freye, R. Haselwimmer, and G. Lonzarich, Nature **394**, 39 (1998).
¹⁰ F. Steglich, B. Buschinger, P. Gegenwart, M. Lohmann, R. Helfrich, C. Langhammer, P. Hellmann, L. Donnevert, S. Thomas, A. Link, et al., J. Phys.: Condens. Matter **8**, 9909 (1996).
¹¹ G.-M. Zhang and L. Yu, Phys. Rev. B **62**, 76 (2000).
¹² S. Capponi and F.F. Assaad, Phys. Rev. B **63**, 155114 (2001).
¹³ J. Jaklic and P. Prelovsek, Adv. Phys. **49**, 1 (2000).
¹⁴ K. Haule, J. Bonca, and P. Prelovsek, Phys. Rev. B **61**, 2482 (2000).
¹⁵ Y. Luo, C. Verdozzi, and N. Kioussis, Phys. Rev. B **71**,

¹⁶ 033304 (2005).

G.-M. Zhang, Q. Gu, and L. Yu, Phys. Rev. B **62**, 69 (2000).

¹⁷ I. Zerec, B. Schmidt, and P. Thalmeier (2006), Physica B, in press; Proceedings of SCES'05.